Observed near-inertial kinetic energy in the northwestern South China Sea

Gengxin Chen,[1] Huijie Xue,[1,2] Dongxiao Wang,[1] and Qiang Xie[1,3]

Received 28 March 2013; revised 21 August 2013; accepted 22 August 2013; published 4 October 2013.

[1] Based on more than 3 years of moored current-meter records, this study examined seasonal variability of near-inertial kinetic energy (NIKE) as well as all large (greater than one standard deviation from the mean) NIKE events related to storms and eddies in the northwestern South China Sea. The NIKE in the subsurface layer (30–450 m) exhibited obvious seasonal variability with larger values in autumn (herein defined as August, September, and October). All large NIKE events during the observation period were generated by passing storms. Most of the NIKE events had an *e*-folding timescale longer than 7 d. The phase velocity, vertical wavelength, and frequency shift of these events were examined. The maximum NIKE, induced by typhoon "Neoguri," was observed in April 2008. Normal mode analysis suggested that the combined effects of the first four modes determined the vertical distribution of NIKE with higher NIKE below 70 m but lower NIKE from 30 to 70 m. Another near-inertial oscillation event observed in August 2007 had the longest *e*-folding timescale of 13.5 d. Moreover, the NIKE propagated both upward and downward during this event. A ray-tracing model indicated that the smaller Brunt-Väisälä frequency and the stronger vertical shear of horizontal currents in an anticyclonic eddy and the near-inertial wave with larger horizontal scale facilitated the unusual propagation of the NIKE and the long decay timescale. Although the NIKE originated from wind, the water column structure affected by diverse oceanographic processes contributed substantially to its complex propagation and distribution.

Citation: Chen, G., H. Xue, D. Wang, and Q. Xie (2013), Observed near-inertial kinetic energy in the northwestern South China Sea, *J. Geophys. Res. Oceans*, *118*, 4965–4977, doi:10.1002/jgrc.20371.

1. Introduction

[2] Oscillations about the local inertial frequency are a commonplace feature in the global ocean. The predominant generation mechanism for near-inertial motions is wind forcing [e.g., *Pollard and Millard*, 1970; *D'Asaro*, 1985] by imparting momentum into the surface mixed layer, leading to an ageostrophic flow that subsequently adjusts and radiates waves [*Rossby*, 1937] and contributing to ocean mixing. The global wind work on inertial motions is comparable to the wind work on geostrophic motions [*Alford*, 2001].

[3] *D'Asaro* [1985] showed that wind forcing of inertial motions is caused primarily by the passage of storms such as cold fronts and low pressure systems. The near-inertial wave response to storms is instantaneously generated in the mixed layer, and then gradually propagates into the thermocline, a process lasting many days after the storm [*Qi et al.*, 1995]. Near-inertial currents forced by tropical cyclones are characterized by low order, forced baroclinic modes [*Geisler*, 1970]. Using velocity and temperature profiles acquired in the western Gulf of Mexico, *Shay et al.* [1998] showed that the evolving three-dimensional current structure could be described by linear, near-inertial wave dynamics. Case studies of typhoon-induced near-inertial motions in the South China Sea (SCS) suggest that the central frequency of the near-inertial band presents an obvious blueshift induced by mesoscale eddies [*Sun et al.*, 2011a] or redshift related possibly to Doppler shift and shear flow modulation around the local inertial frequency [*Sun et al.*, 2011b].

[4] The near-inertial motion also exhibits seasonal cycles, and the seasonality varies from place to place. Based on a database of 640 globally distributed moorings, *Alford and Whitmont* [2007] examined temporal and spatial patterns of near-inertial kinetic energy (NIKE) and concluded there is a surface intensified, seasonal cycle in NIKE. Using observations from a group of moorings in the western North Atlantic Ocean, *Silverthorne and Toole* [2009] suggested the NIKE exhibits a strong seasonal cycle with a wintertime maximum and is dominated by

[1]State Key Laboratory of Tropical Oceanography, South China Sea Institute of Oceanology, Chinese Academy of Sciences, Guangzhou, China.
[2]School of Marine Sciences, University of Maine, Orono, Maine, USA.
[3]Sanya Institute of Deep-Sea Science of Engineering, Chinese Academy of Sciences, Sanya, China.

Corresponding author: H. Xue, 164 West Xingang Road, Guangzhou 510301, China. (hxue@maine.edu)

2169-9275/13/10.1002/jgrc.20371

Table 1. The NIOs Observed in the Northwestern SCS Between 2 June 2007 and 9 August 2010[a]

Date	f_e (cph)	P (h)	f_e/f_0	ζ (10^{-6})	C_p (m/h)	$\overline{\lambda}$(m)	T_e (d)	D (m)	Storm	ID
Aug 2007	0.0228	43.7	0.931	−2.7	3.5	154	13.5	310	Nameless	
Apr 2008	0.0262	38.2	1.069	2.1	5.6	214	4.7	430	Neoguri	0801
Aug 2008	0.0243	41.0	0.992	−6.0	5.3	230	9.7	415	Kammuri	0809
Sep 2008	0.0260	38.5	1.060	5.4	8.6	330	7.9	210	Mekkhala & Higos	0816, 0817
Oct 2009	0.0256	39.2	1.045	2.3	5.2	231	8.7	245	Ketsana	0916
Jul 2010	0.0248	40.5	1.012	6.2	7.4	300	7.0	285	Conson & Chanthu	1002, 1003

[a] C_p, ζ, $\overline{\lambda}$, T_e, D, f_0, f_e, and P represent the upward phase velocity, the background vorticity, the vertical wavelength, the *e*-folding timescale, the vertical range of the inertial wave, the local Coriolis frequency, the depth-averaged NIO frequency between 30 m and D, and the corresponding inertial period. ID is the International designation of storm. Note that the "Nameless," the sixth storm in the west pacific, has not an ID.

downward energy propagation. Furthermore, a depth-integrated NIKE model consisting of a wind forcing term and a dissipation term was used to reproduce the order of magnitude of the observed NIKE successfully as well as its seasonal cycle. Derived from surface trajectories of Argo profiling floats, statistics of inertial currents in the North Pacific, North Atlantic, and Southern Ocean suggested the amplitude in summer is greater than that in winter by 15∼25% [*Park et al.*, 2005].

[5] Previous studies suggested that most observed mixed layer inertial oscillations clearly decay within a week (see Table 1 in *Park et al.* [2009]). Both wave radiation and turbulent dissipation contribute to the decay of inertial motions in the mixed layer. *D'Asaro* [1989] showed that the beta effect temporally changes the meridional wave number and accelerates the decay of near-inertial waves. *Balmforth and Young* [1999] pointed out wave propagation plays the dominant role in near-inertial energy decay at the surface. *Elipot et al.* [2010] suggested the faster decay can also be found in high eddy kinetic energy regions. *Zheng et al.* [2006] found the decay rate of the barotropic inertial wave mode is 2.9 times that of the baroclinic wave mode. Using satellite-tracked drifters, *Park et al.* [2009] examined the global distribution of the decay timescale and concluded that the decay timescale increases with latitude in all basins except the North Atlantic and that the decay timescale is less than 5 d in the Pacific between 15 and 30°N.

[6] The transfer of NIKE to the deep ocean can be influenced by vorticity field associated with mesoscale eddies. *Young and Jelloul* [1997] noted that a field of eddies with horizontal scale much smaller than that of the inertial oscillations can greatly increase the vertical propagation rate of the near-inertial energy. *Klein and Smith* [2001] studied the horizontal dispersion of near-inertial oscillations (NIOs) in a mesoscale eddy field and found the prevalence of the trapping regime inside regions of negative relative vorticity. Using a three-dimensional primitive equation numerical model, *Lee and Niiler* [1998] pointed out anticyclonic eddies can act as a chimney, draining near-inertial energy from the surface to the deep ocean. A similar conclusion was also reached by *Zhai et al.* [2005]. *Danioux et al.* [2008] analyzed the 3-D propagation of wind-forced near-inertial motions in a fully turbulent mesoscale eddy field with a primitive equation numerical model and concluded that refraction by the eddy relative vorticity is the main mechanism responsible for the horizontal distortion of the near-inertial motions, which subsequently triggers vertical propagation. Based on observational data and ray-tracing techniques, *Jaimes and Shay* [2010] suggested near-inertial waves are trapped in regions of negative geostrophic relative vorticity where they rapidly propagate into the thermocline. However, near-inertial waves are stalled in upper layers of cyclonic circulations. The frequency of NIOs can also be shifted by the geostrophic mesoscale flow, especially in anticyclonic vorticity regions [*Elipot et al.*, 2010]. Near-inertial waves can even be reflected within an anticyclonic mesoscale eddy [*Byun et al.*, 2010].

[7] The SCS is a semienclosed marginal sea in the western Pacific Ocean. It is connected with the East China Sea in the north through the Taiwan Strait and the western Pacific Ocean through the Luzon Strait in the northeast. The upper layer ocean circulation of the SCS is driven mainly by the East Asian monsoon. A cyclonic circulation can be observed in the northern SCS all year round. In addition, the Kuroshio intrudes into the SCS via the Luzon Strait during all seasons and forms a southwestward slope current [e.g., *Metzger and Hurlburt*, 1996; *Xue et al.*, 2004; *Wang et al.*, 2010]. A strong boundary current exists in the continental slope and flows southward near the Xisha area (Figure 1), where eddies and storms are also frequently observed [e.g., *Chen et al.*, 2011; *Lee et al.*, 2006]. The present study attempts at a systematic investigation of the seasonal characteristics of the NIKE in the northwestern SCS based on long-term moored records in the Xisha area. High NIKE in the subsurface layer from 40 to 300 m related to frequent events of storms and oceanic eddies was then carefully examined.

[8] The paper was organized as follows: section 2 provided some details on the data used in this study; section 3.1 focused on the seasonal characteristics of the NIKE; section 3.2 investigated high NIKE related to storms and paid special attention to the exceptionally high NIKE event in April 2008; and section 3.3 examined the inertial wave affected by an anticyclonic eddy. Finally, the results were summarized in section 4.

2. Data

[9] Velocity records used to calculate the NIKE were obtained from an up-looking RDI Workhorse Long Ranger 75 kHz ADCP deployed at approximately 17.1°N and 110.3°E in the northwestern SCS (see the red triangle in Figure 1). Time series from 2 June 2007 to 9 August 2010 were used in this study. Sampling time interval was set at 30 min or 1 h, which is short enough to record sufficient

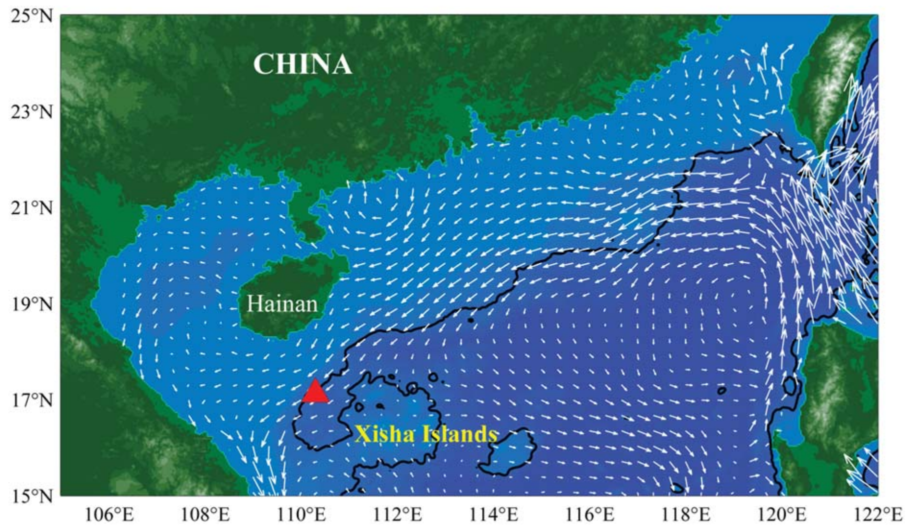

Figure 1. Location of the ADCP mooring station (triangle). Black contours mark the 1000 m bottom depth. The vectors represent the surface geostrophic currents calculated from 18 years of altimeter data.

information on NIOs. The measurements were taken above 450 m with a vertical resolution of 8 m.

[10] According to the instrument specifications, the ADCP echo from a material interface such as the sea surface (when looking up) or sea floor (when looking down) was so much stronger than the echo from scatters in the water that it could overwhelm the side lobe suppression of the transducer. At the 20° beam angle (the situation of our instrument), the last 6% of the measuring range could be contaminated with unpredictable errors, while velocity measurements in the rest 94% depth range had an accuracy of ±1%. In this study, the current velocities were linearly interpolated onto a uniform 5 m interval and the upper 30 m data were excluded from most analyses except in Appendix A, the NIKE in the mixed layer was estimated despite of unsure accuracy of measurements in the top 30 m.

[11] Estimates of the near-inertial horizontal velocity profile (u_i,v_i) were derived from applying a band-pass filter 0.85–1.15 f_0 (similar to *Byun et al*. [2010] and *Xie et al*. [2011]) to the tidal residual, where f_0 is the local Coriolis frequency. The NIKE for each profile was calculated by

$$\mathrm{NIKE} = \frac{1}{2}\rho_0\left(u_i^2 + v_i^2\right) \tag{1}$$

where $\rho_0 = 1024\ \mathrm{kg\ m^{-3}}$ is the reference density.

[12] Storms resulting in larger NIKE at the mooring location were tracked using the best track data set from the Joint Typhoon Warning Center (http://www.usno.navy.mil/NOOC/nmfc-ph/RSS/jtwc/best_tracks/wpindex.html). Daily geostrophic current anomaly derived from the altimeter data (http://www.aviso.oceanobs.com/en/data.html) was used to examine mesoscale eddies. The daily HYCOM + NCODA Global 1/12° Analysis data (http://coastwatch.pfeg.noaa.gov/erddap/griddap/hycom_GLBa008_tdyx.html) was an operational, data-assimilative product and hence was used to substitute for the hydrography that were not measured during the time. The assimilated observations consisted of satellite altimetry and in situ sea surface temperature as well as available in situ vertical temperature and salinity profiles from XBTs, ARGO floats, and moored buoys.

3. Characteristics of NIKE

3.1. Seasonal Characteristics

[13] There existed a seasonal variation of the depth-integrated NIKE (30–450 m; Figure 2a). Higher NIKE was found in autumn (herein defined as August, September, and October), which was mainly contributed by the larger NIKE in August and October. *Alford and Whitmont* [2007] suggested wind was critical to NIKE. *D'Asaro* [1985] showed that wind forcing of inertial motions is caused primarily by the passage of storms. Tropical cyclones in the SCS region occur mainly in July–September [*Lee et al*.,

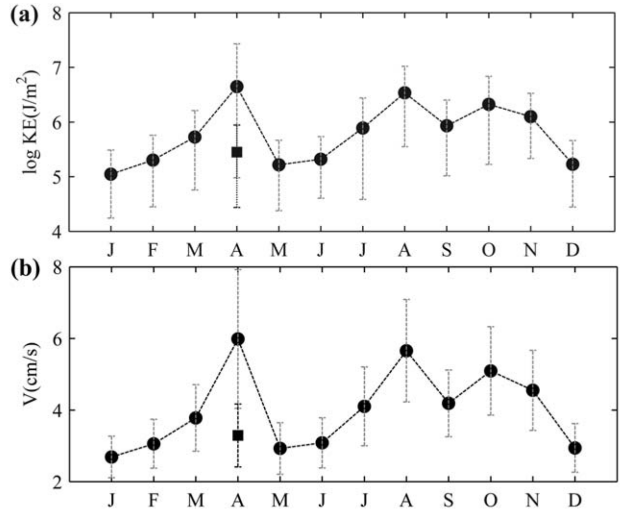

Figure 2. The 30–450 m: (a) depth-integrated NIKE and (b) depth-averaged velocity amplitude. The gray lines represent the upper and lower standard deviation of the average. Squares showed the result without the contribution from 16 to 28 April 2008.

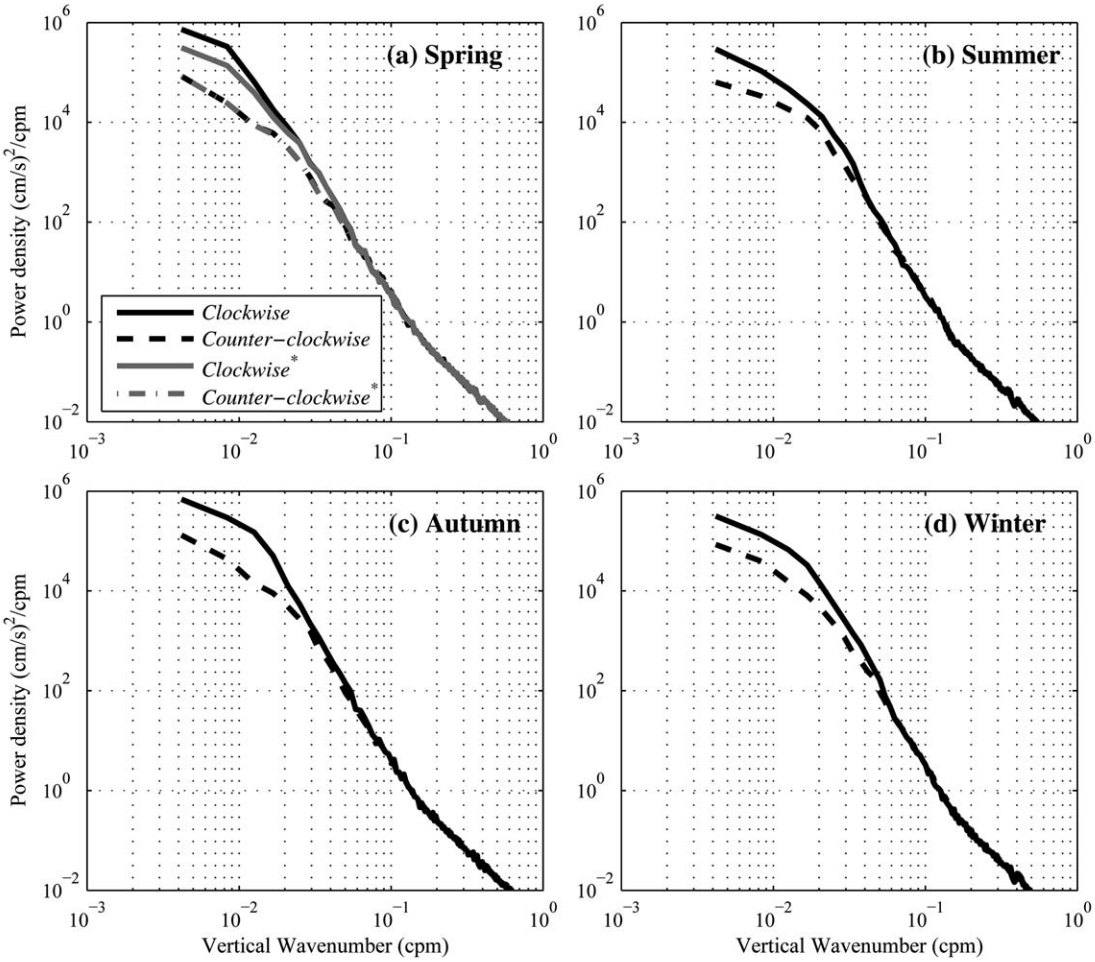

Figure 3. Rotary vertical wave number spectra of the near-inertial velocity profiles showing the clockwise turning with depth component (solid black line) and the counterclockwise component (dashed black line) for (a) spring, (b) summer, (c) autumn, and (d) winter. "Clockwise*" and "Counter-clockwise*" (solid and dashed gray lines in Figure 3a) showed the results without the contribution from 16 to 28 April 2008.

2006], which should have a substantial contribution to the autumn NIKE in the northwestern SCS. Because of the short study period (~3 years), the larger NIKE in April came mainly from the exceptionally high NIKE event induced by typhoon "Neoguri" in April 2008 (see section 3.2), and the NIKE in spring (herein defined as February, March, and April) lowered significantly if the contribution from 16 to 28 April 2008 was excluded (the square in Figure 2a). Although the East Asia monsoon in the SCS was strongest during winter, the NIKE was weaker due to the lack of tropical-storm intensity winds. Besides, the deeper mixed layer in winter, owing to a great loss of the heat on the sea surface [*Liu et al*., 2001], may damp the NIKE. The depth-averaged amplitude of the inertial velocities (Figure 2b) illustrated similar variation as the NIKE. The mean amplitude in 30–450 m layers is about 4.0 cm/s.

[14] The vertical propagation of NIKE was examined using the rotary vertical wave number spectra. Following *Silverthorne and Toole* [2009], several steps were taken to calculate the vertical wavelengths: (i) vertical averages of each horizontal velocity profile were removed; (ii) time averages of horizontal velocity were removed at each depth level; and (iii) velocity was scaled based on the Wentzel-Kramers-Brillouin approximation [*Leaman and Sanford*, 1975]. The near-inertial motions were dominated by clockwise turning (Figure 3), denoting downward energy propagation [*Leaman and Sanford*, 1975]. On vertical scales larger than 100 m, the downward spectral energy was about 7.3 times larger than the upward during autumn. The difference between the downward and upward spectral energy reduced to 3.0 times in winter. In addition, larger NIKE was found in autumn, which was consistent with the results of Figure 2. If the data during 16 to 28 April 2008 was excluded, the upward spectral energy in spring was almost unchanged (Figure 3a). However, the downward spectral energy was only 43% of the situation when all data in spring were reserved. This suggested the typhoon "Neoguri" in April 2008 injected a large fraction of the downward propagating energy to the ocean.

[15] Previous studies suggested that it is difficult for the NIKE generated at the surface to be transferred to the deep ocean without the effect of eddies or storms [*Lee and Niiler*, 1998; *Zhai et al*., 2005]. The obvious seasonal difference of the NIKE vertical distribution in the deeper layer

(Figure 4) suggested that there should be some factors facilitating the propagation of the NIKE into the deeper layer in autumn.

3.2. Larger NIKE in the Deeper Layer

[16] The time evolution of the 40–300 m depth-averaged NIKE is shown in Figure 5. It can be found that the NIKE is lower than the mean value (blue line) most of the time. Only six events did not lie within 1 standard deviation (red dash-dotted line) from the mean. A rough estimate demonstrated the proportion of NIKE induced by the six events reached 42% of the total NIKE over the observation period. Further analysis suggested each high NIKE was accompanied by at least one storm (Table 1 and Figures 5 and 6). However, not every storm induced large NIKE. Taking the situation in 2007 as an example, larger wind speeds induced by "Toraji" and "Lekima" were observed at the mooring location on both 4 July and 2 October 2007 (not shown), whereas no obvious NIKE was found at the same time (Figure 5).

[17] The maximum NIKE during the study period was observed in April 2008, induced by typhoon "Neoguri," and this event was further investigated to illustrate the storm-induced NIOs in the northwestern SCS. Figures 7a and 7b show the time series of inertial current profiles from 16 to 28 April 2008. The magnitude of the oscillation was about 40 cm s^{-1} for both the eastward and northward current components. Based on the slope of the inertial current profiles, the upward phase velocity C_p was estimated to be 5.6 m h^{-1}, signifying a downward energy propagation (Figure 7c). The vertical range (D) of the inertial wave reached deeper than 430 m during "Neoguri," where D is defined as the maximum depth of the horizontal velocity 5 cm s^{-1} (black contours in Figure 7).

[18] An interesting phenomenon is that larger NIKE was found in the deeper layer from 80 to 200 m, but NIKE was low between 30 and 70 m. To understand the penetration of NIKE into the ocean interior, the horizontal near-inertial velocity components, u and v, were expanded in terms of the vertical normal modes [*Danioux et al*., 2008; *Gill*, 1984]:

$$(u, v) = \sum_{n=0}^{\infty} (u_n, v_n)(x, y, t)F_n(z). \tag{2}$$

[19] $F_n(z)$ are the eigenfunctions of the Sturm-Louisville problem [*Flierl*, 1978]:

$$\frac{\partial}{\partial z}\frac{f_0^2}{N^2}\frac{\partial}{\partial z}F_n + \frac{1}{R_n}F_n = 0, \tag{3}$$

$$\frac{\partial F_n}{\partial z} = 0 \quad z = 0, \ -h. \tag{4}$$

[20] Here R_n is the Rossby radius of deformation of mode n; h is the depth of ocean; and N is the Brunt-Väisälä frequency.

[21] Based on the 1/12° daily HYCOM GLBu0.08 data, the time evolution of the Brunt-Väisälä frequency (N_t) at the mooring location is shown in Figure 8a. The weaker N_t in the surface layer during the NIO event (16–28 April 2008) should be attributed to the stronger mixing induced by the typhoon. Meanwhile, the typhoon-induced pumping drove the location of the maximum N_t gradient shallower and stronger (Figure 8).

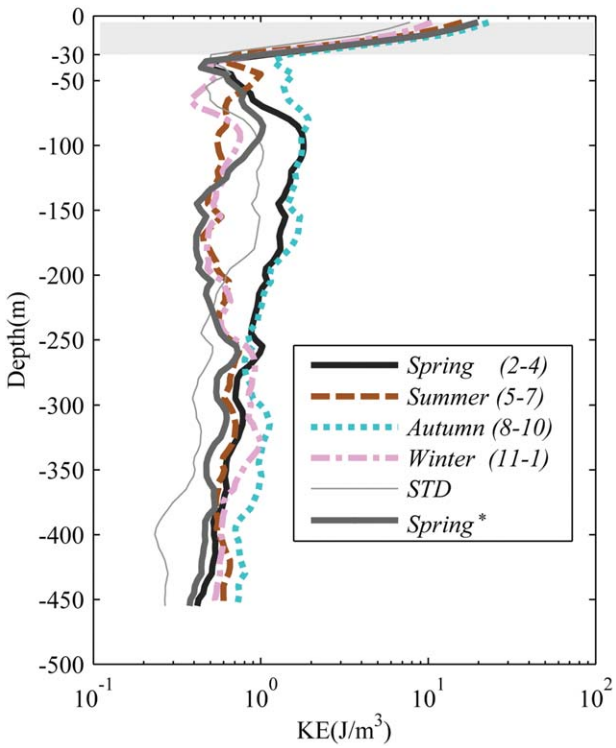

Figure 4. The NIKE vertical distribution in four seasons. The gray line represents the vertical distribution of standard deviation of all the NIKE profiles. "Spring*" means the NIKE distribution in spring without the contribution from 16 to 28 April 2008. The upper 30 m is included to show the recorded velocities there, but it is shaded to indicate there are unquantifiable amount of errors associated with this layer and the corresponding structures should be viewed with caution.

[22] To solve the eigenvalue problem, N in equation (3) was set as the time-averaged N_t from 16 to 28 April 2008. Each R_n corresponded to each $F_n(z)$ and thus each vertical mode. Figure 9a shows the time-averaged NIKE profiles for the first four baroclinic modes ($n = 1$, 2, 3, and 4). The sum of modes 1–4 (black line in Figure 9a) revealed the general characteristics of NIKE shown in Figure 9b. The stronger NIKE in the deeper layer (i.e., 150 m; Figures 7c and 9b) was mainly captured by the higher vertical modes (modes 2–4), whereas the larger NIKE in the surface layer deduced from general principles should be largely contributed by the first baroclinic mode. These results suggest that the depth-varying stratification plays an important role in the penetration of NIKE into the ocean interior for effect of the stratification on the lower mode ($n = 1$) differs from those on higher modes ($n = 2$, 3, and 4) because of their different Rossby radii of deformation R_n. Since the pattern of NIKE aligned with that of the first four modes, one could expect the group velocity of these modes to dictate how NIKE propagated vertically. The inertial wave corresponding to the first mode usually propagated faster than the

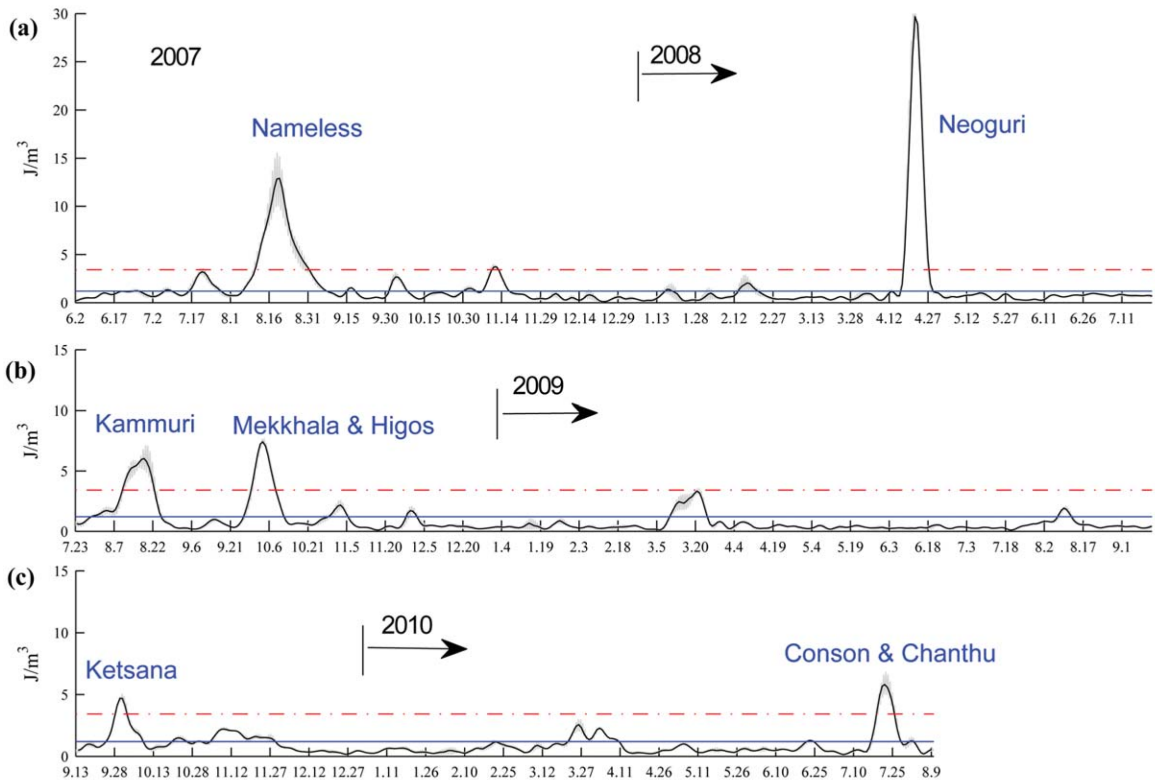

Figure 5. The time evolution of the 40–300 m depth-averaged hourly (gray line) and daily (black line) NIKE. The blue solid line and the red dash-dotted line represent the mean value and the upper 1 standard deviation, respectively. The horizontal axis represents date in month.day from 2 June 2007 to 9 August 2010.

other higher modes because of its longer vertical wavelength. It quickly left the observation area but the rest higher modes stayed at the location longer. Because of that, the NIKE in the deeper layer dominated by the higher modes appeared later but maintained longer (Figure 7c).

[23] Spectral analysis was applied to the time series of tidal residual currents during 16–28 April 2008 at all levels from 30 to 450 m (Figure 10). The dashed line and dash-dotted lines represent the local inertial frequency f_0 and the $0.85f_0$ and $1.15f_0$, respectively. There was an obvious power concentration in near-inertial frequency band, especially at 70–250 m. The near-inertial frequency increased with depth (Figure 10), which suggests that the NIO converted its energy to higher frequency movement and participated in deep ocean mixing. The mean of the NIKE peak frequency from the upper 430 m, f_e, was 0.0262 cph, which was 7% higher than the local inertial frequency. With the vertical phase velocity of 5.6 m h^{-1} mentioned above (Figure 7), the vertical wavelength was about 214 m.

[24] Inertial motions were generated within a few hours of typhoon passage, but decayed over a few days, much longer than the generation timescale [*Park et al*., 2009].

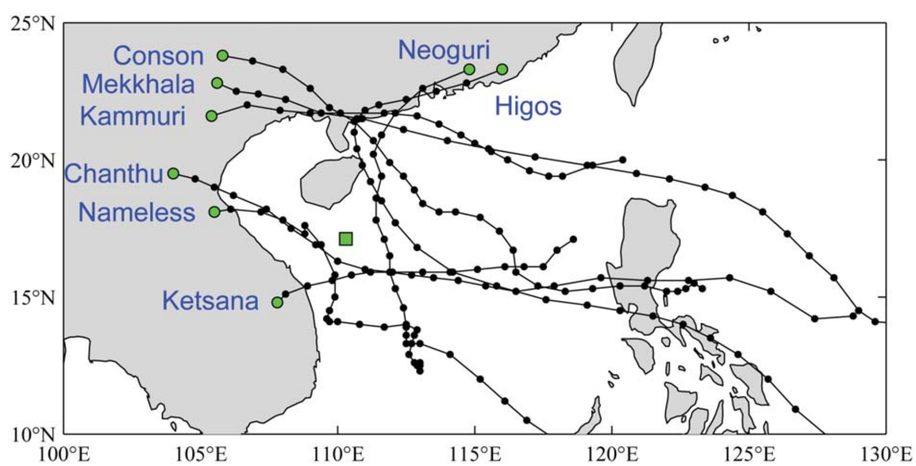

Figure 6. Six hourly storm tracks. The green square denotes the location of the ADCP mooring.

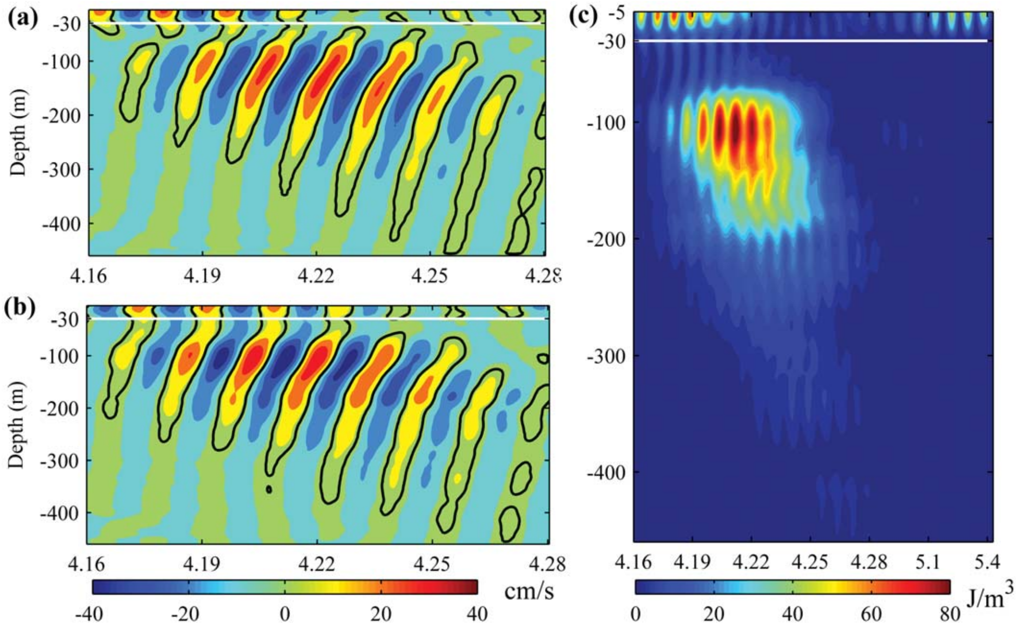

Figure 7. Time series of the (a) eastward and (b) northward component of the inertial current from 16 to 28 April 2008. Black contours mark the velocity of 5 cm s^{-1}. (c) Time evolution of NIKE. Because of the unpredictable errors associated with velocity measurements in the upper 30 m, distributions in this layer (above the white line) should be viewed with caution.

Based on the time series of the 40–300 m depth-averaged NIKE, herein, the *e*-folding timescale T_e determined from the NIKE temporal autocorrelation function was regarded as the decay timescale of the inertial motion generated by storm forcing. Thus, the decay timescale of the NIKE induced by Neoguri was 4.7 d. Note that the timescale was not sensitive to the data length (Figure 11) because random signals are not correlated with each other, and thus have little contribution to the correlation function.

[25] Similar analysis was applied to other NIO events shown in Figure 5, and the results were listed in Table 1. The oscillation frequency f_e was not exactly the local inertial frequency f_0. Most NIOs had a frequency slightly above f_0, except two events occurred in August 2007 and August 2008, respectively (Table 1). Previous investigation by *Kunze* [1985] revealed that the background flow vorticity would modify the NIO frequencies such that

$$f_e = f_0 + \zeta/2 \tag{5}$$

in which ζ was the background vorticity. Although the f_e in Table 1 was not identical to the estimation using equation (5), the background vorticity during the NIO events in

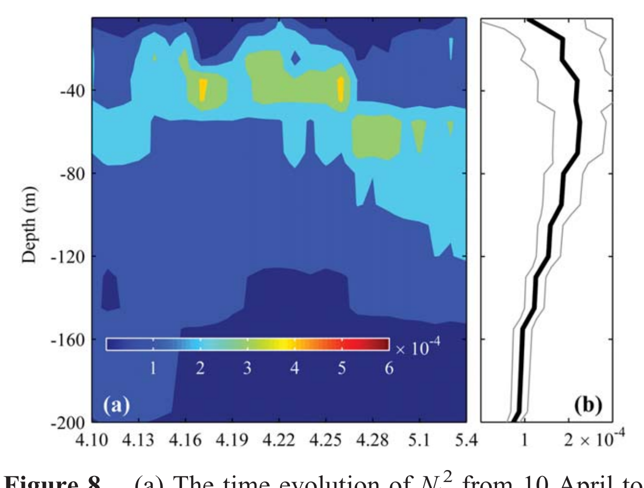

Figure 8. (a) The time evolution of N_t^2 from 10 April to 4 May 2008 (unit: s^{-2}). (b) The mean N_t^2 (thick line). The thin lines represent the upper and lower standard deviation of the average.

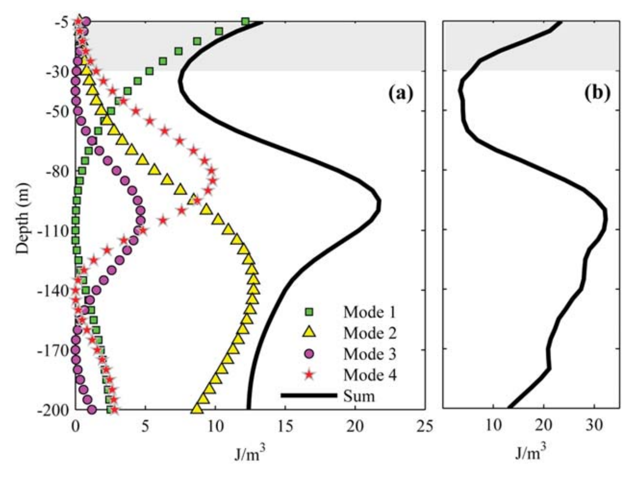

Figure 9. (a) The time-averaged NIKE for the first four baroclinic modes ($n = 1$, 2, 3, and 4) and the combination of these four modes. (b) The time-averaged NIKE from 16 to 28 April 2008. Because of the unpredictable errors associated with velocity measurements in the upper 30 m, the NIKE in this layer (shaded) should be viewed with caution.

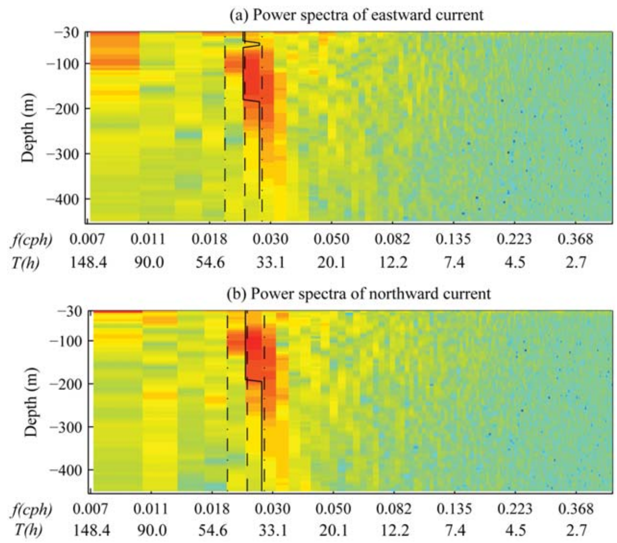

Figure 10. Power spectra of (a) eastward and (b) northward current components at all depths. The dash line and dash-dotted lines represent the local inertial frequency f_0, 0.85 f_0, and 1.15 f_0, respectively. The solid line denotes the peak near-inertial frequency, f_e.

August 2007 and August 2008 was indeed negative, whereas the background vorticity was positive during other events (not shown). The decay timescales of the NIKE in 40–300 m layer were all larger than 7 d except for the "Neoguri" case, which was different from the finding that the decay timescale is generally less than 5 d in the mixed layer [*Park et al*., 2009]. The discrepancy might have originated from the alien hydrological characteristics in different regions and the NIKE in the deeper layer was dominated by higher modes that lasted longer. In addition, the decay timescales of the two events in August 2007 and August 2008 were longer compared to other events. Further

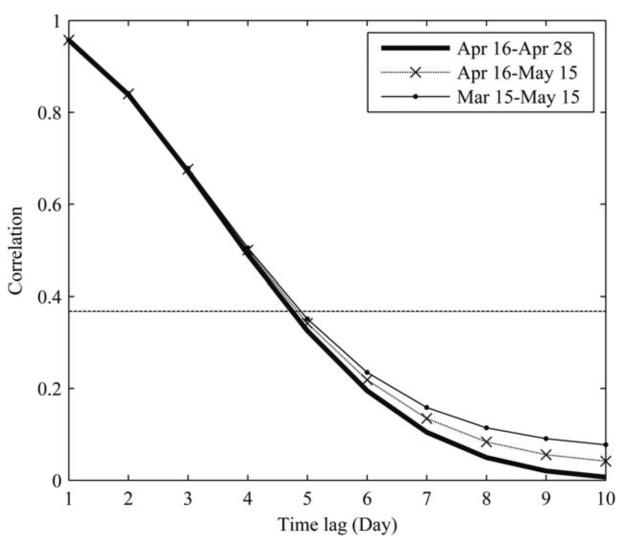

Figure 11. The temporal autocorrelation functions of the 40–300 m depth-averaged NIKE from 16 to 28 April 2008, from 16 April to 15 May 2008, and from 15 March to 15 May 2008. The horizontal line represents the value of $1/e$.

analysis suggested that the two NIO events were also affected by anticyclonic eddies (see section 3.3). The event in August 2007 was more special, which had not only the longest decay timescale of 13.5 d, but also a large frequency shift that was about 7% lower than f_0 (Table 1).

3.3. Inertial Waves in an Anticyclonic Eddy

[26] Eddies are frequently observed in the Xisha area, including locally generated and propagated from the northeastern regions along the continental slope [*Chen et al*., 2011]. Both the altimeter data and HYCOM GLBu0.08 data show an anticyclonic eddy in the Xisha area in August 2007 (Figure 12). Due to the impact of this eddy, the background vorticity at the mooring station was negative until 7 September 2007 (Figure 13b), when the NIKE finally faded away (Figure 13a).

[27] The NIOs in August 2007 were generated by a "Nameless" storm passing around 6 August 2007. Subsequently, the NIKE in the subsurface layer gradually

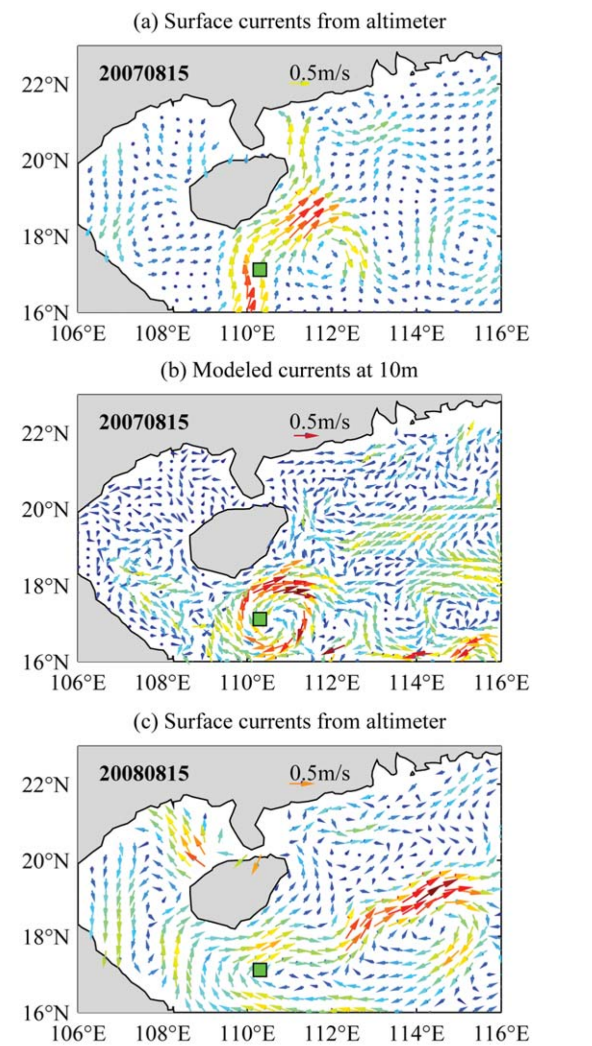

Figure 12. (a) The geostrophic currents anomaly from the altimeter data on 15 August 2007, (b) the modeled currents at 10 m depth on 15 August 2007 from HYCOM GLBu0.08, and (c) same as Figure 12a, except for 15 August 2008.

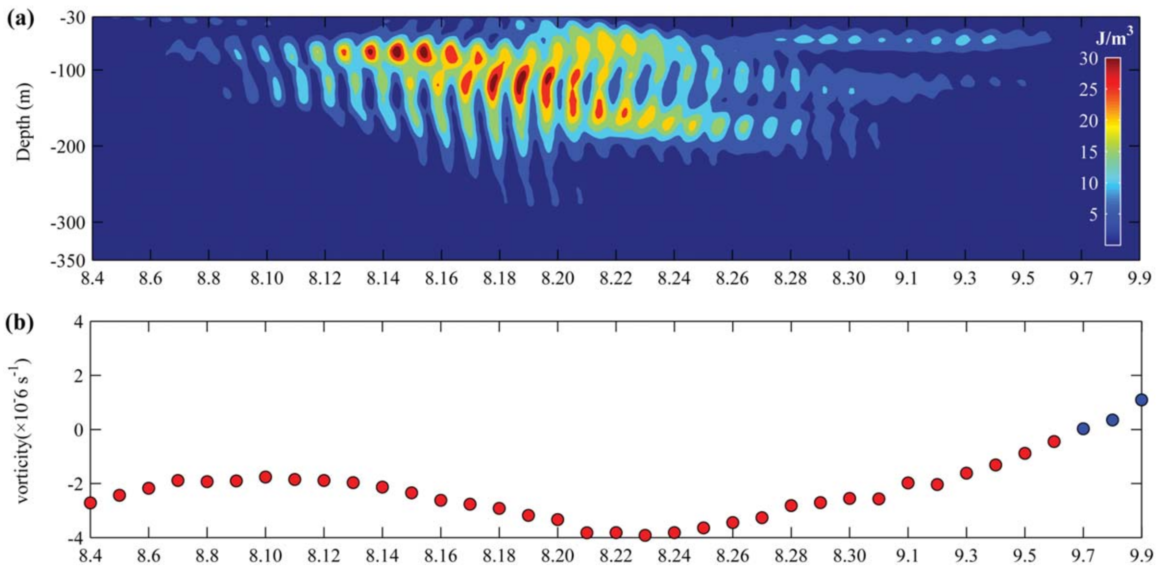

Figure 13. (a) Time evolution of NIKE for the NIO event in August 2007 and (b) the background vorticity at the mooring station obtained from satellite data during the same period.

intensified until 20 August. After that, the NIKE began to decrease and eventually faded away in early September (Figure 13a). Compared with the NIOs induced by the typhoon "Neoguri," the NIKE generated by the "Nameless" storm was weaker with a maximum value of only 30 J m^{-3}. The propagation depth of the inertial waves was also shallower, about 310 m. The near-inertial frequency increased with the depth and had a larger redshift in frequency, especially at depth of 35–70 m with the frequency about 13% lower than the f_0 (Figure 14). Two special phenomena were noted. One was that the NIOs lasted for around 1 month. The other was that the NIKE propagated both upward and downward between 14 and 22 August (Figure 13a). Considering that the "Nameless" storm did not occupy the mooring area longer than other storms (Figure 6) (in fact, it made landfall on 9 August 2007), the longer decay timescale should be attributed to other factors than the storm itself.

[28] Similar to the situation in April 2008, the N_t in the surface layer was also weaker in August 2007. However, the location of the maximum N_t gradient significantly deepened to about 120 m during the NIO event (Figure 15),

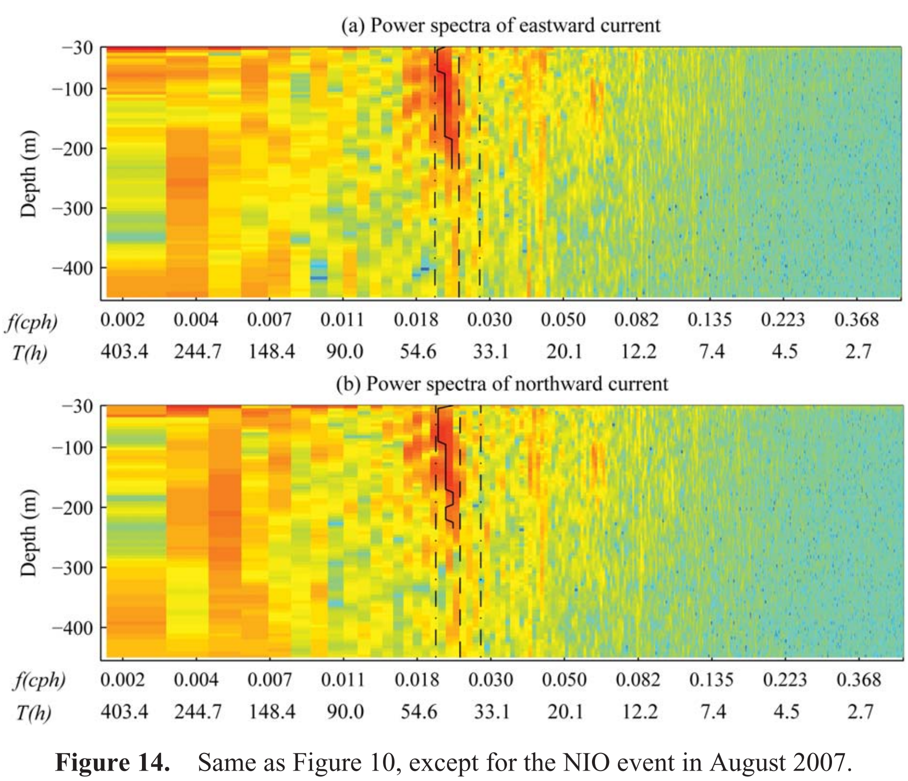

Figure 14. Same as Figure 10, except for the NIO event in August 2007.

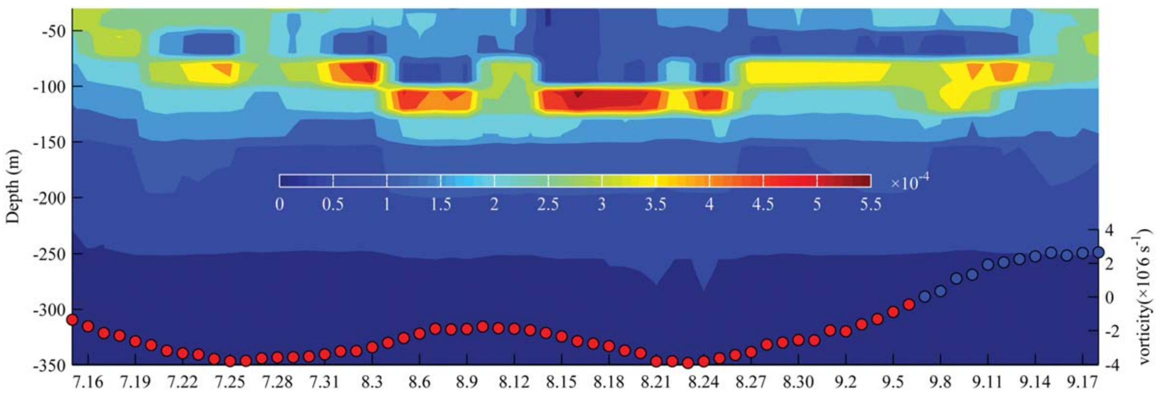

Figure 15. Similar to Figure 8a except for the period from 15 July to 18 September 2007. Dots denote the background vorticity at the same time.

which was totally different from the shallow situation during the "Neoguri" event (Figure 8). Previous studies suggested that an anticyclonic eddy in the SCS can cause the thermocline to deepen considerably [*Chen et al.*, 2010, 2011]. Thus, the deeper location of the maximum N_t gradient during the NIO event should be attributed to the effect of the aforementioned anticyclonic eddy.

[29] The ray-tracing model of *Kunze* [1985] can explore the propagation of near-inertial waves in flow field (see formulas in Appendix B). It connects the wave position with the velocity shear and stratification but neglects the energy exchange between waves and mean flow. The model was successfully applied to track near-inertial waves by *Byun et al*. [2010] and *Jaimes and Shay* [2010]. It was also used in this study to further explore the effects of the anticyclonic eddies on the NIO. Due to the limit of the mooring data, only the vertical component of this model was used. In the model, $k_x = k_y$ and the horizontal wavelength in zonal direction (λ_x) was a constant 40 km, taken from *Shcherbina et al*. [2003] based on the observations in another marginal sea—the Japan Sea; the initial value of the vertical wavelength was 120 m; $\zeta = 0.1\ f_0$; N varied vertically and temporally as seen from Figure 15; and U and V were the hourly observed currents, low-pass filtered with a cutoff period of 4 days as in *Byun et al*. [2010]. The ray tracing began at 50 m.

[30] Lines in Figure 16 are the paths of the near-inertial waves. The unusual upward waves were observed during 13–22 August 2007, agreeing reasonably well with the observed upward propagation of NIKE. Two other values of λ_x equal to 50 and 100 km were also examined. More upward waves were observed in the first case, whereas all waves propagated upward in the second one (not shown). Obviously, the waves with larger horizontal wavelength tended to propagate upward. Moreover, if λ_x was 40 km or 100 km or even 500 km but the waves were tracked starting at a depth of 120 m, no upward waves could be observed, which denoted the effect of the velocity shear and stratification. Furthermore, the reciprocal of the gradient Richardson number

$$R_g = \frac{\sqrt{(\partial U/\partial z)^2 + (\partial V/\partial z)^2}}{N^2} \tag{6}$$

is shown in Figure 16 (color). The upward near-inertial waves (black lines in Figure 16) appeared in the high R_g regions, suggesting that the smaller N_t and the stronger vertical shear of horizontal currents in the anticyclonic eddy facilitated the unusual upward propagation of the near-inertial waves. Previous studies suggested that most of the inertial events even with larger horizontal wavelength have

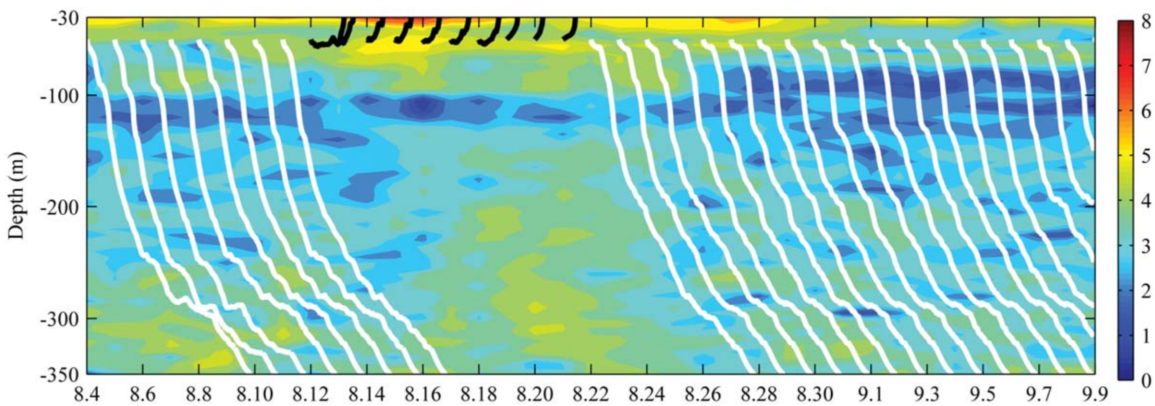

Figure 16. Paths of the near-inertial waves (black and white lines) and time evolution of $\ln(R_g)$ (color). Paths were tracked using the hourly velocities, whereas R_g was computed using daily velocities.

the energy propagate downward, which should be attributed to that R_g was not high enough. *Byun et al*. [2010] provided the first observational evidence of reflection within the seasonal thermocline and thermostad of an anticyclonic mesoscale eddy. If the high R_g regions alternated in the depth, the near-inertial waves with proper horizontal wavelength could be reflected and trapped in special layers. Due to the lack of observed hydrography, the daily modeled Brunt-Väisälä frequency was used in the present study. In reality, vertical shears of the horizontal velocity combined with more complex Brunt-Väisälä frequency changes could lead to more complex wave paths and thus result in longer decay time scales because of wave reflection, reduced vertical velocity, and so on. In addition, the near-inertial frequency increased with the depth (Figure 14), suggesting the wave with larger frequency (generally smaller wavelength) was more advantageous to propagate downward. This verified that the upward wave was more likely to have larger wavelength as mentioned above. With larger R_g, both upward and downward NIKE related to inertial waves with different wavelengths due to frequency dispersion could be observed during 14–22 August.

[31] The August 2008 event was also affected by an elliptic anticyclonic eddy (Figure 12c). Compared with the event in August 2007, the mooring located farther to the eddy center. The stratification at the mooring location, especially during the NIO event, was not strongly affected by the eddy (not shown). It is thus concluded that having the long persistence of NIKE requires the collocation of storm and eddy.

4. Summary

[32] Oscillations about the local inertial frequency are a commonplace feature in the global ocean and contribute greatly to oceanic mixing. Due to insufficient observation data, investigations of near-inertial energy in the SCS have been limited. In this study, the seasonal variability of kinetic energy from near-inertial motions was determined. High NIKE in the subsurface layer from 40 to 300 m related to storms and oceanic eddies was then carefully examined.

[33] The NIKE below 40 m depth exhibited an obvious seasonal variability. On the seasonal average, the largest NIKE was found in autumn. Although the East Asia monsoon in the SCS was strongest during winter, the NIKE was weaker due to the deeper mixed layer and the fact that the wind in winter seldom reaches the intensity of tropical storms. An usual feature was that the NIKE was larger below 250 m than that above 250 m in summer and winter (Figure 4a), which may be attributed to that some inertial oscillation events dominated by the higher modes holding larger amount of energy in deeper layer and the lower modes with larger surface expression dispersing faster.

[34] Every instance of high NIKE in the 40–300 m layer was accompanied by at least one storm, showing that the generation of large NIKE can primarily be attributed to the passage of storms. Most NIOs during the period from 2 June 2007 to 9 August 2010 had a vertically averaged peak frequency slightly above f_0, but two events (in August 2007 and August 2008) stood out with the frequency below f_0 due to the effect of negative background vorticity. The maximum NIKE was observed in April 2008. During this event, high NIKE was found in layers deeper than 70 m but not in the subsurface layer from 30 to 70 m. Normal mode analysis suggested that the strong NIKE from 70 to 430 m was mainly captured by vertical modes 2–4, whereas the NIKE in the surface layer should be largely contributed by the first baroclinic mode.

[35] Most NIOs had a decay timescale less than 10 d except one induced by the "Nameless" storm in August 2007. The *e*-folding timescale of this NIO event was 13.5 d. Moreover, the NIKE propagated both upward and downward. This perhaps represents an observational evidence of the "chimney effect," which describes the trapping of near-inertial waves in an anticyclonic eddy. A ray-tracing model indicated that the small Brunt-Väisälä frequency and the strong vertical shear of horizontal currents in an anticyclonic eddy and the near-inertial wave with large horizontal scale were beneficial to the unusual propagation of the NIKE and the longer decay timescale.

[36] Our results suggested the NIKE presented various vertical structures and was not simply monotonically decreasing with the depth. Although NIKE originated from wind, the water column structure affected by diverse oceanographic phenomena substantially contributed to the propagation path, decay timescale, vertical distribution of the NIKE. Sometimes a weaker storm could induce stronger NIKE and longer decay timescale, and thus exerted important influence on the ocean.

Appendix A: The Upper 30 m Velocity Measurements

[37] As the last 6% of the measuring range could be contaminated, the upper 30 m velocity measurements were discarded in this study. However, considering that the upper 30 m data may provide additional information on NIOs in the northwestern SCS, Figures 4, 7, and 9 were drawn to include the upper 30 m even though we were unable to assure the accuracy of the data. *Chaigneau et al*. [2008] found the near-inertial amplitudes off the east coast of China to be as large as 20 cm s^{-1}. Here, the time-averaged NIKE in the mixed layer shown in Figure 4 was the order of 10 J m^{-3}, which corresponded to near-inertial amplitudes of 14 cm s^{-1}.

[38] Both Figures 4 and 7 suggested that the larger velocity could be found in the surface layer and deeper layer but not the subsurface layer (e.g., 30 m depth). This phenomenon could also be verified during the August 2007 event (not shown). Thus, the weaker NIKE in the subsurface layer may be a common feature in the southwestern SCS. Figure 9 suggested the stronger NIKE in the deeper layer was mainly captured by the higher vertical modes, whereas the NIKE in the surface layer was largely contributed by the first baroclinic mode. As the higher modes usually propagated slower, the NIKE in the deeper layer may have longer decay timescale and affected the ocean more persistently.

[39] The monthly, integrated NIKE from the mixed layer could be estimated by

$$\mathrm{NIKE}_{ML} = \frac{1}{2}\rho_0 \int_0^H \left(u_z^2 + v_z^2\right) \mathrm{d}z.$$

[40] Here, H is the mixed-layer depth, which was defined using temperature step $\Delta T = 0.8°\mathrm{C}$ from near-surface

temperature based on the WOA09 data [*Kara et al.*, 2000]. The averaged $NIKE_{ML}$ was estimated to be 289 J m^{-2}. The NIKE in the whole water column (0–450 m) was about 638 J m^{-2}. Therefore, the NIKE in deeper layer was 349 J m^{-2}, which was even larger than the $NIKE_{ML}$. This result suggested the $NIKE_{ML}$ was likely underestimated due to the uncertainty in velocity measurements in the top 30 m. The actual NIKE in the surface layer could be higher than that shown in Figure 7c.

Appendix B: The Ray-Tracing Model of *Kunze* [1985]

[41] In the model, the wave position $\mathbf{r} = (r_x, r_y, r_z)$ and the wave number $\mathbf{K} = (k_x, k_y, k_z)$ were governed by

$$\frac{d\mathbf{r}}{dt} = \mathbf{Cg} + \mathbf{Vg} \tag{B1}$$

and

$$\frac{d\mathbf{K}}{dt} = -\nabla\omega. \tag{B2}$$

[42] Here $\mathbf{Cg} = (Cg_x, Cg_y, Cg_z)$ is the group velocity of the near-inertial wave, and its vertical component is given by

$$Cg_z = \frac{\partial\omega_0}{\partial k_z} \approx \frac{-N^2 k_H^2}{f{k_z}^3} - \frac{1}{k_z^2}\left(\frac{\partial U}{\partial z}k_y - \frac{\partial V}{\partial z}k_x\right), \tag{B3}$$

where ω_0 is the intrinsic frequency of the near-inertial wave. $\mathbf{Vg} = (U, V)$ is the geostrophic flow; N is the Brunt-Väisälä frequency, and the dispersion relation is

$$\omega = f_e + \frac{N^2 k_H^2}{2f k_z^2} + \frac{1}{k_z}\left(\frac{\partial U}{\partial z}k_y - \frac{\partial V}{\partial z}k_x\right) + \left(\mathbf{K}\cdot\mathbf{V}_g\right) = \text{const}. \tag{B4}$$

[43] In this study, the meridional wavelength ($\lambda_y = 2\pi/k_y$) is set to equal the zonal wavelength ($\lambda_x = 2\pi/k_x = 40$ km), and the vertical wavelength is chosen to be 120 m. The ray-tracing results can be affected by many parameters. For example, if the vertical wavelength is larger than 280 m in the situation of $\lambda_x = 40$ km, no upward propagating waves can be observed. However, if a larger λ_x of 100 km is used, both upward and downward waves can be observed again for the vertical wavelength of 280 m. The pattern of alternating upward and downward phase propagation of inertial waves can still be observed sometimes even when $k_x \neq k_y$, e.g., $\lambda_x = 30$ km and $\lambda_x = 48$. These results suggest that the ray-tracing solution provides only a qualitative explanation because the accurate value of parameters cannot be assigned based on the data from a single mooring. However, the model provides intuitive results of the alternating upward and downward phase propagation of inertial waves, and it clearly suggests the effects of vertical shear and stratification on inertial waves.

[44] **Acknowledgments.** Insightful comments from Willi Rath and another anonymous reviewer are very helpful in improving the work. This work is supported by National Basic Research Program of China (grant 2011CB403504 and 2011CB403503), the Guangzhou City Project for the Pearl River New Star in Science and Technology (grant 2013J2200087), and National Natural Science Foundation of China (grant 41106027 and 41206008).

References

Alford, M. H. (2001), Internal swell generation: The spatial distribution of energy flux from the wind to mixed layer near-inertial motions, *J. Phys. Oceanogr.*, *31*(8), 2359–2368.

Alford, M. H., and M. Whitmont (2007), Seasonal and spatial variability of near-inertial kinetic energy from historical moored velocity records, *J. Phys. Oceanogr.*, *37*(8), 2022–2037.

Balmforth, N., and W. Young (1999), Radiative damping of near-inertial oscillations in the mixed layer, *J. Mar. Res.*, *57*(4), 561–584.

Byun, S. S., J. J. Park, K. I. Chang, and R. W. Schmitt (2010), Observation of near-inertial wave reflections within the thermostad layer of an anticyclonic mesoscale eddy, *Geophys. Res. Lett.*, *37*, L01606, doi:10.1029/2009GL041601.

Chaigneau, A., O. Pizarro, and W. Rojas (2008), Global climatology of near-inertial current characteristics from Lagrangian observations, *Geophys. Res. Lett.*, *35*, L13603, doi:10.1029/2008GL034060.

Chen, G., Y. Hou, and X. Chu (2011), Mesoscale eddies in the South China Sea: Mean properties, spatiotemporal variability, and impact on thermohaline structure, *J. Geophys. Res.*, *116*, C06018, doi:10.1029/2010JC006716.

Chen, G., Y. Hou, Q. Zhang, and X. Chu (2010), The eddy pair off eastern Vietnam: Interannual variability and impact on thermohaline structure, *Cont. Shelf Res.*, *30*(7), 715–723.

D'Asaro, E. A. (1985), The energy flux from the wind to near-inertial motions in the surface mixed layer, *J. Phys. Oceanogr.*, *15*(8), 1043–1059.

D'Asaro, E. A. (1989), The decay of wind-forced mixed layer inertial oscillations due to the β effect, *J. Geophys. Res.*, *94*, 2045–2056.

Danioux, E., P. Klein, and P. Rivière (2008), Propagation of wind energy into the deep ocean through a fully turbulent mesoscale eddy field, *J. Phys. Oceanogr.*, *38*(10), 2224–2241.

Elipot, S., R. Lumpkin, and G. Prieto (2010), Modification of inertial oscillations by the mesoscale eddy field, *J. Geophys. Res.*, *115*, C09010, doi:10.1029/2009JC005679.

Flierl, G. R. (1978), Models of vertical structure and the calibration of two-layer models, *Dyn. Atmos. Oceans*, *2*(4), 341–381.

Geisler, J. E. (1970), Linear theory of the response of a two layer ocean to a moving hurricane, *Geophys. Fluid Dyn.*, *1*, 249–272.

Gill, A. (1984), On the behavior of internal waves in the wakes of storms, *J. Phys. Oceanogr.*, *14*(7), 1129–1151.

Jaimes, B., and L. K. Shay (2010), Near-inertial wave wake of hurricanes Katrina and Rita over mesoscale oceanic eddies, *J. Phys. Oceanogr.*, *40*(6), 1320–1337.

Kara, A., P. A. Rochford, and H. E. Hurlburt (2000), An optimal definition for ocean mixed layer depth, *J. Geophys. Res.*, *105*, 16,803–16,821.

Klein, P., and S. L. Smith (2001), Horizontal dispersion of near-inertial oscillations in a turbulent mesoscale eddy field, *J. Mar. Res.*, *59*(5), 697–723.

Kunze, E. (1985), Near-inertial wave propagation in geostrophic shear, *J. Phys. Oceanogr.*, *15*(5), 544–565.

Leaman, K. D., and T. B. Sanford (1975), Vertical energy propagation of inertial waves: A vector spectral analysis of velocity profiles, *J. Geophys. Res*, *80*, 1975–1978.

Lee, C. S., Y. L. Lin, and K. K. W. Cheung (2006), Tropical cyclone formations in the South China Sea associated with the mei-yu front, *Mon. Weather Rev.*, *134*(10), 2670–2687.

Lee, D. K., and P. P. Niiler (1998), The inertial chimney: The near-inertial energy drainage from the ocean surface to the deep layer, *J. Geophys. Res.*, *103*, 7579–7591.

Liu, Q., Y. Jia, P. Liu, Q. Wang, and P. Chu (2001), Seasonal and intraseasonal thermocline variability in the central South China Sea, *Geophys. Res. Lett.*, *28*, 4467–4470.

Metzger, E. J., and H. E. Hurlburt (1996), Coupled dynamics of the South China Sea, the Sulu Sea, and the Pacific Ocean, *J. Geophys. Res.*, *101*, 12,331–12,352.

Park, J. J., K. Kim, and B. A. King (2005), Global statistics of inertial motions, *Geophys. Res. Lett.*, *32*, L14612, doi:10.1029/2005GL023258.

Park, J. J., K. Kim, and R. W. Schmitt (2009), Global distribution of the decay timescale of mixed layer inertial motions observed by satellite-tracked drifters, *J. Geophys. Res.*, *114*, C11010, doi:10.1029/2008JC005216.

Pollard, R. T., and R. Millard Jr. (1970), Comparison between observed and simulated wind-generated inertial oscillations, *Deep Sea Res. Oceanogr. Abstr.*, *17*(4), 153–175.
Qi, H., R. A. De Szoeke, C. A. Paulson, and C. C. Eriksen (1995), The structure of near-inertial waves during ocean storms, *Collections*, *25*, 2583–2871.
Rossby, C. (1937), On the mutual adjustment of pressure and velocity distributions in certain simple current systems, *J. Mar. Res.*, *1*(19), 239–263.
Shay, L. K., A. J. Mariano, S. D. Jacob, and E. H. Ryan (1998), Mean and near-inertial ocean current response to Hurricane Gilbert, *J. Phys. Oceanogr.*, *28*(5), 858–889.
Shcherbina, A. Y., L. D. Talley, E. Firing, and P. Hacker (2003), Near-surface frontal zone trapping and deep upward propagation of internal wave energy in the Japan/East Sea, *J. Phys. Oceanogr.*, *33*(4), 900–912.
Silverthorne, K. E., and J. M. Toole (2009), Seasonal kinetic energy variability of near-inertial motions, *J. Phys. Oceanogr.*, *39*(4), 1035–1049.
Sun, L., Q. Zheng, D. Wang, J. Hu, C. K. Tai, and Z. Sun (2011a), A case study of near-inertial oscillation in the South China Sea using mooring observations and satellite altimeter data, *J. Oceanogr.*, *67*(6), 1–11.
Sun, Z., J. Hu, Q. Zheng, and C. Li (2011b), Strong near-inertial oscillations in geostrophic shear in the northern South China Sea, *J. Oceanogr.*, *67*(4), 377–384.
Wang, D., B. Hong, J. Gan, and H. Xu (2010), Numerical investigation on propulsion of the counter-wind current in the northern South China Sea in winter, *Deep Sea Res., Part I*, *57*(10), 1206–1221.
Xie, X. H., X. D. Shang, H. van Haren, G. Y. Chen, and Y. Z. Zhang (2011), Observations of parametric subharmonic instability-induced near-inertial waves equatorward of the critical diurnal latitude, *Geophys. Res. Lett.*, *38*, L05603, doi:10.1029/2010GL046521.
Xue, H., F. Chai, N. Pettigrew, D. Xu, M. Shi, and J. Xu (2004), Kuroshio intrusion and the circulation in the South China Sea, *J. Geophys. Res.*, *109*, C02017, doi:10.1029/2002JC001724.
Young, W., and M. B. Jelloul (1997), Propagation of near-inertial oscillations through a geostrophic flow, *J. Mar. Res.*, *55*(4), 735–766.
Zhai, X., R. J. Greatbatch, and J. Zhao (2005), Enhanced vertical propagation of storm-induced near-inertial energy in an eddying ocean channel model, *Geophys. Res. Lett.*, *32*, L18602, doi:10.1029/2005GL023643.
Zheng, Q., R. Lai, N. Huang, J. Pan, and W. Liu (2006), Observation of ocean current response to 1998 Hurricane Georges in the Gulf of Mexico, *Acta Oceanol. Sin.*, *25*(1), 1–14.